Threshold Behavior in the Initiation of Hippocampal Population Bursts

Liset Menendez de la Prida,[1,2,*] Gilles Huberfeld,[1] Ivan Cohen,[1,3] and Richard Miles[1]
[1] INSERM U739
CHU Pitié-Salpêtrière
Université Pierre et Marie Curie
Paris 75013
France
[2] Neurobiología-Investigación
Hospital Ramón y Cajal
Madrid 28034
Spain

Summary

Hippocampal population discharges such as sharp waves, epileptiform firing, and GDPs recur at long and variable intervals. The mechanisms for their precise timing are not well understood. Here, we show that population bursts in the disinhibited CA3 region are initiated at a threshold level of population firing after recovery from a previous event. Each population discharge follows an active buildup period when synaptic traffic and cell firing increase to threshold levels. Single-cell firing can advance burst onset by increasing population firing to suprathreshold values. Population synchrony is suppressed when threshold frequencies cannot be reached due to reduced cellular excitability or synaptic efficacy. Reducing synaptic strength reveals partially synchronous population bursts that are curtailed by $GABA_B$-mediated conductances. Excitatory glutamatergic transmission and delayed $GABA_B$-mediated signals have opposing feedback effects on CA3 cell firing and so determine threshold behavior for population synchrony.

Introduction

Brain function depends on the coordinated activity of large populations of neurons. Distinct behavioral states are associated with the generation of population discharges such as the theta and gamma rhythm (Bragin et al., 1995; Buzsaki et al., 1983; Leung, 1992; Traub et al., 1996; Somogyi and Klausberger, 2005; Steriade, 2005). Synchronous population discharges characterize specific stages of development (Ben-Ari, 2001; Garaschuk et al., 2000). Excessive synchrony in specific brain regions is the signature of various pathological states including the epilepsies (Jefferys, 1994) and Parkinson disease (Levy et al., 2000).

Two distinct types of interaction seem to underlie the expression of these population activities. Fast oscillations such as the theta and gamma rhythms depend on temporally patterned interactions between functionally opposing signals mediated by principal cells and GABAergic interneurons. Another type of population discharge, including the hippocampal sharp waves (Buzsaki, 1986), interictal discharges (Ayala et al., 1973; Schwartzkroin and Prince, 1978), and rhythmic activities during development (Ben-Ari et al., 1989), recurs at longer and more variable intervals. The second type of activity is generated by functionally excitatory interactions that act to synchronize neuronal firing into periodic population bursts (Miles and Wong, 1987; Traub and Wong, 1982; Traub and Miles, 1991).

The factors that determine the timing of periodic population events are not well understood. Evidently, cellular excitability and synaptic efficacy must recover from a previous burst. Hyperpolarizing synaptic events (Alger and Nicoll, 1980; Hablitz, 1984) and cellular potentials dependent on Ca^{2+}-dependent K^+ channels and the I_h current (Agmon and Wells, 2003) probably terminate too quickly to control the timing of a succeeding population burst. Instead, it has been suggested that the recurrent excitatory synapses that synchronize cellular discharges (Miles and Wong, 1987) also control the duration of intervals between them. Transmitter release from these synapses is reduced after a population burst due to depression and other factors. Synaptic function must recover before another burst can be initiated in hippocampal (Staley et al., 1998) and spinal cord population activities (Fedirchuk et al., 1999; Staley et al., 1998, 2001). According to this logic, the interval between population events should depend exclusively on the time course of vesicle replenishment (Bains et al., 1999; Staley et al., 1998, 2001; Tabak et al., 2001).

Alternatively, population events may be initiated by active processes that involve synaptic transmission of activity within the population after recovery is complete (Calvin, 1972; Chamberlin et al., 1990; Ives and Jefferys, 1990; Traub and Dingledine, 1990). Such mechanisms may imply that a burst is initiated when a threshold frequency of synaptic or cellular activity is exceeded (Menendez de la Prida and Sanchez-Andres, 1999, 2000; Wenner and O'Donovan, 2001), but firm evidence on this point requires precise measurements of activity within the cell population responsible for burst initiation.

Here, we examined population activity during the initiation of population bursts in the CA3 region of the hippocampus when fast inhibition was suppressed. This activity depends on cellular interactions within a neuronal population small enough to be adequately recorded with several extracellular electrodes. We combined single-cell and multiunit records with computational analysis to compare contributions of recovery and active threshold processes to the timing of population burst initiation. We show that recovery over a period of several seconds after a burst determines when the next population burst can occur, but its precise timing depends on threshold behavior. Population bursts are preceded by an active buildup period, during which glutamatergic and delayed $GABA_B$-mediated signals compete to drive pyramidal cells toward or away from synchronous firing. Threshold behavior for population burst firing thus shares some

*Correspondence: liset.m.prida@hrc.es
[3] Present address: Division of Neuroscience, Baylor College of Medicine, Houston 77030, Texas.

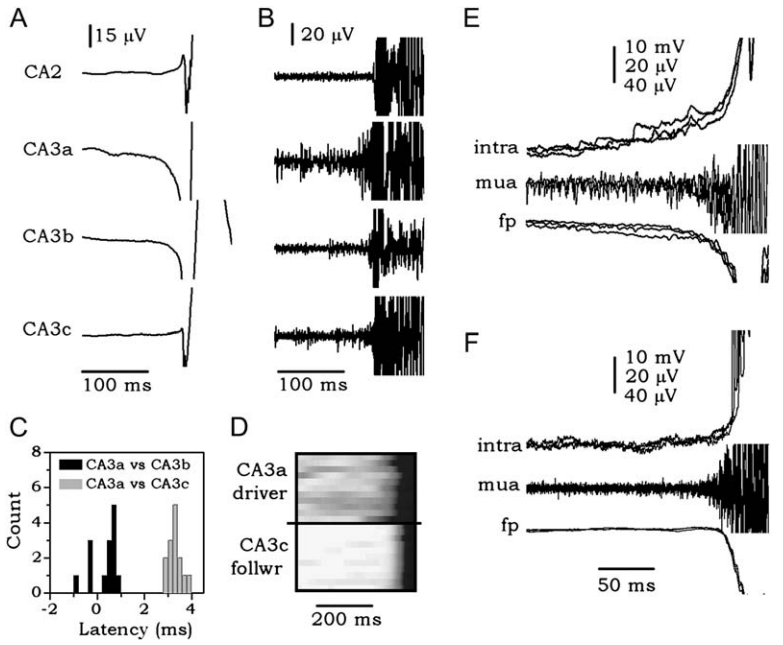

Figure 1. Spatial Dynamics of Population Events in CA3 Disinhibited Minislices

(A) Field potentials, filtered at 0.1–100 Hz, recorded from four tungsten electrodes at different CA3 regions.

(B) Multiunit activity, derived by filtering between 100 Hz and 10 kHz the same records.

(C) Cross-correlation analysis showing latencies between the different CA3 regions in one typical experiment calculated using the CA3a signal as reference. A positive latency in the cross-correlation with the CA3b signal means that CA3a signals precede, while a negative latency means that they follow firing in the CA3b signal.

(D) Firing rate from 11 consecutive episodes triggered by the event onset. White to black scale shows the cascade of firing preceding population bursts at driver but not at follower sites.

(E) EPSPs recorded from a CA3a cell correlated with the buildup of multiunit activity (mua) and the extracellular negative deflection in the local field.

(F) Cells recorded from the CA3c follower region showed little synaptic activity preceding population events.

features with that for action potential generation in a single neuron.

Results

Driver and Follower Sites in the Initiation of Population Events in the CA3 Region

Population discharges were generated repetitively in minislices of the CA3 region exposed to the $GABA_A$ receptor antagonist picrotoxin (PTX; 100 μM; n = 78). We examined their initiation using tungsten electrodes placed in the s. pyramidale, which record the spiking activity of a local population of several hundred cells (Cohen and Miles, 2000). Field potentials were derived by low-pass filtering (Figure 1A). High-pass filtering was used to record multiunit activity (Figure 1B). At a separation of 200 μm, two electrodes record from nonoverlapping cell populations (see Experimental Procedures and Figure S1 in the Supplemental Data available with this article online).

We found that electrodes in the CA3a region detected the first activity of each synchronous event. Synchronous activity in other areas of the CA3 region had a delayed onset (Colom and Saggau, 1994; Knowles et al., 1987; Traub and Wong, 1982). Cross-correlation of field potentials showed that the CA3b and CA3c signals followed the CA3a signal with latencies of 0.9 ± 0.4 ms and 3.8 ± 0.9 ms, respectively (n = 22; Figure 1C). These data suggest that cells of the CA3a region drive the initiation of synchronous bursts and the other regions are follower sites. A consideration of the size of the region, ~600 μm, and the thickness of slices, 400 μm, together with cell soma diameter, 20 μm, and packing density of three cells within the s. pyramidale suggests that the CA3a driver area contains about 1800 to 2000 cells. Thus, three extracellular electrodes can record the firing of most, possibly all, of the cells involved in generating population events (Cohen and Miles, 2000).

Cellular and Field Mechanisms Underlying Driver and Follower Dynamics

Records from driver and follower sites revealed differences in multiunit firing and field potentials preceding population events. An increase in firing began 50–150 ms before synchronous bursts at driver but not at follower sites (Figure 1B). This was particularly evident when several consecutive events were aligned by their onset. Figure 1D, which compares 11 events from one experiment at the driver (CA3a) and follower (CA3c) sites, depicts the cascade of firing preceding the event onset at the driver region alone.

In field potentials from driver sites, a negative deflection was correlated with the increase of population firing before a population burst. At follower sites, there was either no deflection or a small positive deflection starting less than 10 ms before the local population burst (Figure 1A). The firing rate in the CA3a region during the buildup period was negatively correlated with the latency of events between CA3a and the follower site in CA3c ($r^2 = 0.6$; $p < 0.0001$). This suggests that the spread of activity depends on firing in the CA3a driver region.

Intracellular sharp records from cells located in driver and follower sites revealed differences in synaptic activity just before population bursts. In 12 of 14 cells recorded from the driver zone, an increase in EPSP frequency was correlated with the buildup of multiunit firing and the field potential deflection (Figure 1E). EPSPs occurring during the buildup period summed into a slow depolarization with similar time course to the extracellular deflection (intracellular: 20 ± 11 ms; field: 23 ± 8 ms; n = 12; not significantly different, p = 0.587; Figure 1E). Synaptic activity during the buildup period was also observed from whole-cell records in voltage-clamp mode, which permitted an improved discrimination of EPSCs (n = 5 cells; see below and Figure 3F).

In cells from the follower region, population events occurred abruptly with little or no increase in EPSP frequency (n = 7 cells; Figure 1F). This difference between

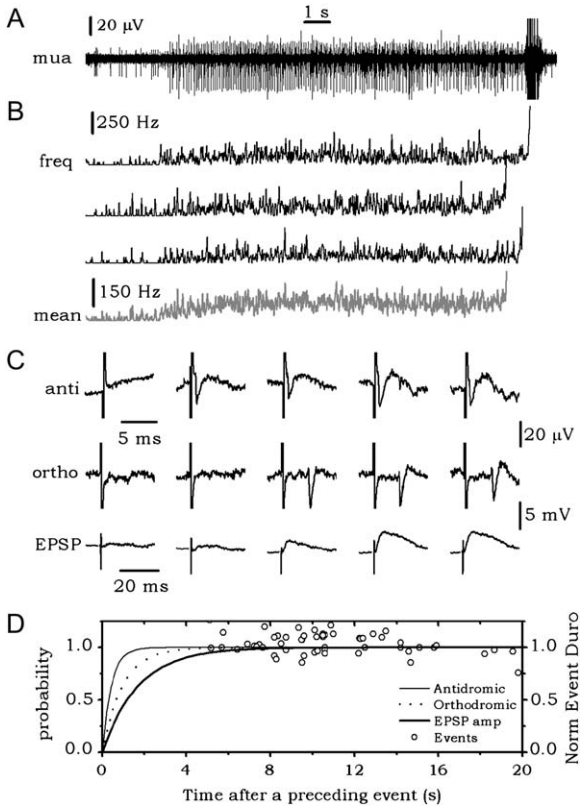

Figure 2. Time Course of Changes in Cellular and Synaptic Processes between Population Bursts

(A) Multiunit activity (mua) and (B) firing rate derived from multiunit records was reduced to a minimum after a population event and recovered to stable but fluctuating plateau. A sudden buildup in firing to a threshold level preceded the onset of the next event. Black traces are examples from three consecutive episodes, and gray traces are their mean. (C) Recovery dynamics of orthodromic and antidromic units and EPSPs. Traces from left to right are taken from time points in the ranges 0–150 ms, 200–350 ms, 550–700 ms, 2500–3000 ms, and 4000–4500 ms after the termination of a preceding event. (D) Summary of the recovery probability of antidromic spikes, orthodromically activated action potentials, and EPSP amplitude. Open dots show the distribution of intervals between population events.

driver and follower cells did not derive from differences in their time constants, which were similar ($p = 0.101$): 15 ± 5 ms for driver cells (n = 12) and 12 ± 3 ms for follower cells (n = 7). We suggest that the increased synaptic activity is due to the increase in firing of the recurrently connected CA3 pyramidal cell population and generates the field potential associated with the onset of a synchronous event.

Cellular and Synaptic Changes throughout Activity Cycle

We next examined how burst initiation was related to the recovery from a preceding event in records from the CA3a region. Since population firing depends on both cellular excitability and synaptic efficacy (Cohen and Miles, 2000), multiunit activity provides a global view of recovery processes in the CA3 region (Figure 2A). Plotting the frequency of all spikes detected by an extracellular electrode against time after a preceding event (Figure 2B), showed that the interval between events could be divided into three parts. They were (1) a recovery period, (2) a plateau period, and (3) a buildup period. After a burst, firing rate dropped to minimum. The recovery period was defined as the period for firing rate to return to levels prior to a burst. This process followed exponential dynamics with a time constant of 2410 ± 430 ms (n = 22 minislices; see Figure S2). A plateau period of variable duration (3.9–20 s) began when firing returned to preburst frequencies. During this period, firing rate fluctuated with increases and decreases around a maintained level (Figure 2B). It was terminated by the onset of the buildup period. This period was identified from the increased firing frequency and field potential deflection prior to burst onset and had duration of 71 ± 20 ms (Figure 2B). Firing frequencies at the end of the buildup period appeared to be higher than at any other point during the cycle (Figure 2B).

We further examined recovery of cellular and synaptic properties by examining extra- and intracellular responses to focal stimulation. Low intensity stimuli applied at 1–2 Hz near the alveus could antidromically activate single units in records from the s. pyramidale of the CA3a region. Antidromic spikes, which provide an index of cellular excitability, were initiated with a short, invariant latency and could follow stimulation at 50 Hz. Figure 2C shows that antidromic units recovered completely at 511 ± 325 ms after population bursts at interval of 3.9–7.3 s (data from five to seven consecutive cycles from n = 9 units; Figure S2).

Orthodromic spikes, with longer latencies and higher failure probabilities, could also be elicited by stimulation near the alveus. These events provide data on the recovery of both synaptic efficacy and EPSP-spike coupling after a preceding population burst. The probability to elicit an orthodromic spike of similar amplitude and form recovered at 1023 ± 375 ms in slices with a mean interval between bursts of 3.9–7.3 s (data from five to seven consecutive cycles from n = 9 units; Figure 2C and Figure S2).

We also examined the recovery of EPSPs elicited by alvear stimulation using sharp recordings (Figure 2C). EPSP amplitude recovered at 2034 ± 1232 ms (n = 6 cells; Figure S2). Voltage-clamp data from patch recordings showed that EPSC amplitude recovered with a similar time course (n = 4 cells; Figure S2).

Figure 2D summarizes these results. It shows that population bursts (dots) are initiated after recovery of cellular and synaptic indices is completed (solid and dashed lines). In neuronal systems where recovery processes dominate initiation processes (Grzywacz and Sernagor, 2000; Staley et al., 2001; Tabak et al., 2001), the duration of an event is correlated with the preceding interevent interval. We found that these parameters were poorly correlated for population bursting recorded in the presence of 4 mM K^+ ($r^2 = 0.3 \pm 0.2$; n = 7 minislices).

Conditions for the Initiation of Population Activity in Driver Sites

If cellular and synaptic indices were fully recovered by the time of burst onset, then the timing of these events may depend on distinct processes. We next examined events occurring after recovery. In all cases, firing

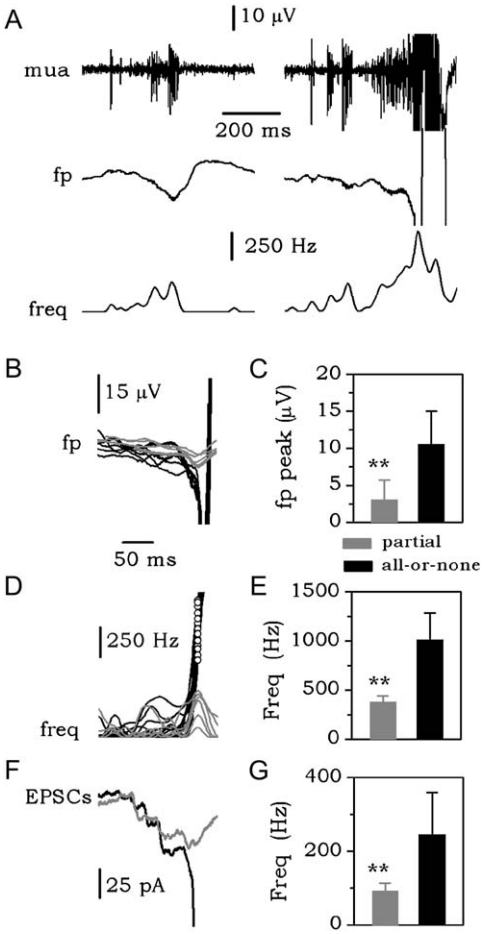

Figure 3. Comparison of Partial and All-or-None Events

(A) Comparison of multiunit activity, field potential, and spike frequency during partial (left) and all-or-none (right) events. (B) Field potential deflections during partial (gray) and all-or-none (black) events were triggered for comparison. (C) Negative deflections associated with partial events were smaller than those during buildup periods preceding all-or-none bursts (**p < 0.0001). Data from five consecutive episodes from n = 22 minislices. (D) Firing frequency changes during partial (gray) and all-or-none (black) events. Dots mark the firing rate threshold at the onset of all-or-none events for each individual trace. (E) Firing frequency during partial events was lower than that immediately preceding all-or-none bursts (**p < 0.0001). Data from five consecutive episodes from n = 22 minislices. (F) EPSCs recorded during partial (gray) and all-or-none (back) events. (G) EPSC frequency during partial events was lower than firing increases during the buildup period preceding burst onset (**p < 0.001). Data from 10 to 12 episodes from n = 5 cells. Error bars represent the mean ± SDM.

frequencies at the end of the buildup period appeared to be higher than any other fluctuation occurring during the plateau period.

We compared firing frequency during the plateau and the buildup periods. The mean firing rate at the driver sites during the plateau period was 44 ± 22 Hz (n = 22 minislices). Close examination revealed transient increases in firing at the driver region. The larger fluctuations were associated with field potentials consisting of a negative deflection followed by a positive wave as seen during the buildup period (Figure 3A). These events apparently correspond to partially synchronous population bursts—some, but not all, cells fire nearly simultaneously (Traub and Miles, 1991; Wenner and O'Donovan, 2001). We compared the firing increase and field potentials associated with all-or-none and partial events from field-triggered data segments. Field potential deflections preceding population events were significantly larger than those associated with partial events ($p < 0.0001$; Figures 3B and 3C). Firing increases associated with partial events were also smaller than those occurring before all-or-none population discharges ($p < 0.0001$; Table 1 and Figures 3D and 3E). At the event onset, defined at the start of the first population spike, the firing rate at driver regions reached a maximum of 1010 ± 276 Hz (n = 22 minislices). This value was higher than at any other point during the period between bursts, suggesting that bursts are initiated when a threshold firing frequency is exceeded. We defined the firing frequency at the burst onset as the threshold frequency for the initiation of population events (Figure 3D, dots).

Table 1 summarizes the conditions for event onset at driver sites with 4 mM extracellular potassium. Since automatic spike detection may underestimate high firing frequencies due to overlapping spikes (see Experimental Procedures and Figure S3), we also estimated the firing frequency in the 10 ms period before event onset by visual spike detection. This gave slightly higher estimates of the threshold frequency of 1179 ± 246 Hz (n = 22). Both automatic detection and visual counts showed that firing frequency at the onset of all-or-none bursts exceeded that of the largest partial population events (Table 1; $p < 0.0001$).

We also examined the frequency of EPSCs converging on single CA3a pyramidal cells during the buildup period in whole-cell recordings (Figure 3F). As for firing frequency, we found that the EPSC frequency was considerably higher during the buildup period, 246 ± 113 Hz, than during any transient increase during the plateau period (92 ± 22 Hz; $p = 0.017$; data from 10 to 12 episodes from n = 5 cells; Figure 3G).

Changes in Cellular Excitability Did Not Affect Frequency Threshold for Population Events

These results suggest that population bursts may be initiated when activity in the CA3a driver region exceeds a threshold. CA3 population activity depends on both cellular excitability and recurrent excitatory synaptic interactions. We next asked how changing these two parameters affected the occurrence and the threshold for the generation of population discharges.

Cellular excitability was modified by changing the extracellular K^+ concentration in the presence of PTX (n = 7 minislices). The multiunit firing rate recorded during the plateau period increased with K^+ over the range 2–8 mM (Figure 4A, white bars). Population burst firing was never observed in 2 mM K^+; it occurred in two out of seven minislices at 3 mM and in all experiments at 4, 6, and 8 mM (Figure 4A, black bars). Reducing K^+ from 8 mM to 2 mM always suppressed population burst firing. This demonstrates that cellular excitability must exceed a certain level to generate population discharges.

As shown in Figure 4B, increasing K^+ in the range of 4–8 mM reduced the interval between population bursts but did not change the duration of the buildup period or

Table 1. Effect of Different Extracellular Concentrations of K^+ and 0.2 – 0.7 μM NBQX

	Extracellular K^+			+NBQX
	4 mM (22)	6 mM (7)	8 mM (7)	0.2 – 0.7 μM (6)
Interevent period				
Duration (s)	6.1 ± 3.3	5.3 ± 2.1	3.1 ± 2.3	8.2 ± 3.8
Mean firing rate (Hz)	44 ± 22	53 ± 19	66 ± 17	93 ± 54
Transients (Hz)	381 ± 64	294 ± 56	317 ± 64	592 ± 193
Buildup period				
Duration (ms)	71 ± 20	68 ± 19	77 ± 25	107 ± 25
Threshold frequency (Hz)				
Automatic detection	1010 ± 276	966 ± 153	916 ± 112	1311 ± 319
Spike counting	1179 ± 246	1178 ± 373	1184 ± 259	1719 ± 309

Numbers in parentheses indicate the number of slices. Data are given as mean ± SDM.

the threshold frequency (Table 1). The temporal evolution of firing rate during the buildup period is shown here for three consecutive events at 4, 6, and 8 mM K^+ in one representative slice. The threshold firing frequency (open dots in Figure 4B) did not change significantly over this range of K^+. In contrast, the interevent interval was consistently reduced. Firing rate values during partial events were similar at different K^+ concentrations (Table 1).

The reduction of the interevent interval at higher K^+ resulted from shorter plateau periods (Figure 4C, left). The recovery dynamics were comparable in 4 and 6 mM K^+ (Figure 4C, right). At 6 mM, as at 4 mM K^+, burst duration was not correlated with the interval between the preceding (r^2 = 0.3 ± 0.1; n = 7; Figure 4D, filled dots) or the following population event (r^2 = 0.1 ± 0.1; open dots). In contrast, at 8 mM K^+, burst duration was better correlated with the preceding interval (r^2 = 0.6 ± 0.1; n = 7; Figure 4D and inset, filled dots) but not with the following interval (r^2 = 0.2 ± 0.1; open dots). The recovery time constant was smaller compared with 4 and 6 mM (Figure 4C, right). All this suggests that recovery processes become more important when burst interval is reduced by increasing cellular excitability. Even so, the buildup period preceding population bursting was little changed in these conditions.

Contribution of Synaptic Activity to Threshold Initiation of Population Events

We used 3-dihydroxy-6-nitro-7-sulfamoyl-benzo(f)-quinoxaline-2,3 dione (NBQX), which blocks AMPA and kainate receptors, to examine the effects of reducing excitatory synaptic efficacy on the initiation of synchronous events. NBQX at concentrations of 2–2.5 μM completely suppressed spontaneous population bursts induced by 100 μM PTX in the presence of 4 mM K^+ (n = 4 minislices). At lower concentrations (0.2–0.7 μM; n = 9), population bursts were not suppressed, but the interval between them was increased (Table 1; Figure 5A). NBQX increased the threshold firing frequency for burst initiation and the duration of the buildup period (Table 1). The recovery dynamics of multiunit firing was comparable in control and NBQX (Figure 5B).

Another change observed in low concentrations of NBQX was a consistent increase of the number of partial events (240% ± 90%; n = 9 minislices). As in control conditions, they consisted of a negative-positive field potential correlated with a increase in unit firing (Figures 5C and 5D and Table 1). Intracellularly, they were associated with a depolarizing potential (1.2 ± 0.6 mV; n = 9 cells) succeeded by a hyperpolarization of 3.7 ± 2.8 mV at resting potential (Figure 5C), which reversed at −85 ± 6 mV. This reversal potential suggests that the hyperpolarization that terminates partial population events might be mediated by the activation of $GABA_B$ receptors.

Role of $GABA_B$-Mediated Neurotransmission in Sculpting Partial Events

We pursued the role of $GABA_B$ receptors in the termination of partial population events. To this end, we wished to compare the time course of glutamatergic and $GABA_B$ conductances with population firing. A procedure developed by Borg-Graham (Borg-Graham et al., 1998; Borg-Graham, 2001) allows estimation of the time course of conductances (ΔG) and the composite reversal potential (*Vrev*) from complex synaptic events recorded at several different membrane potentials. We performed this analysis using data from both sharp (current-clamp data; n = 3 cells) and whole-cell (voltage-clamp data; n = 3) recordings.

Conductance changes were examined with respect to the onset of partial events defined from field potentials. This analysis revealed increases of ΔG during partial events associated with changes of *Vrev* from the resting potential to a peak of −31 ± 6 mV at 15–20 ms after the onset. At 125–270 ms, *Vrev* hyperpolarized to −81 ± 5 mV (Figure 5E). Separating contributions of excitatory and inhibitory conductances showed that the initial depolarization was due to the activation of excitatory conductances. They were curtailed by a rise of inhibitory conductances starting at 39 ± 19 ms after the onset of excitation and reaching a peak at 240 ± 96 ms (Figure 5E). We noted that multiunit firing was strongly reduced as the inhibitory conductance increased. Plotting the instantaneous firing rate as a function of the rising phase of both the excitatory and the inhibitory conductances clearly demonstrated this correlation (Figure 5F).

If the activation of $GABA_B$ receptors, due to interneuron firing, curtails partial population events, then suppressing this signaling might restore all-or-none bursts. We tested this prediction by applying the $GABA_B$ receptor antagonist CGP52432 (2–5 μM; n = 8 minislices) in the presence of NBQX (0.4–0.7 μM). After adding CGP, the

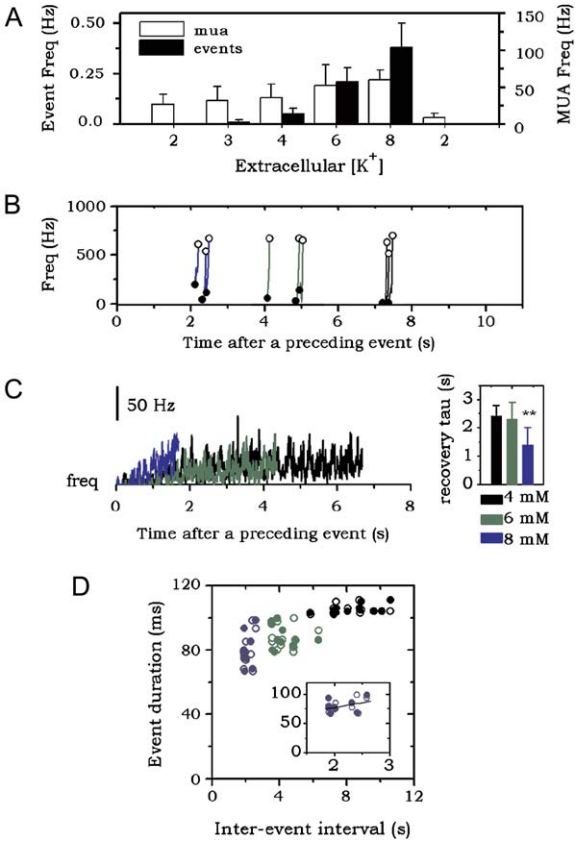

Figure 4. Effect of Changes in Cellular Excitability

(A) Effect of changes in the extracellular potassium concentration on the mean firing rate (white bars) and the frequency of all-or-none population bursts (black bars). (B) Firing rate during the buildup period plotted on a timescale corresponding to the cycle between bursts. The filled circle corresponds to the firing frequency preceding the buildup, and the open circle corresponds to that at the onset of the event. Increasing K^+ concentration from 4 mM to 8 mM significantly decreased the interevent interval and so increased event frequency. Data from three successful events in each condition obtained from the same experiment. (C) Left: Average frequencies of multiunit firing at 4 mM (black), 6 mM (green), and 8 mM K^+ (blue) during a cycle in a typical experiment. Note that the duration of the recovery period was reduced at 8 mM K^+ (**$p < 0.0001$) but that recovery time constants were similar at 6 mM and 4 mM K^+ (right; data from n = 7 minislices). (D) Event duration versus the preceding (filled dots) and the following (open dots) interevent interval for different concentrations of K^+ in one representative experiment. Inset highlights the case of 8 mM K^+. Error bars represent the mean ± SDM.

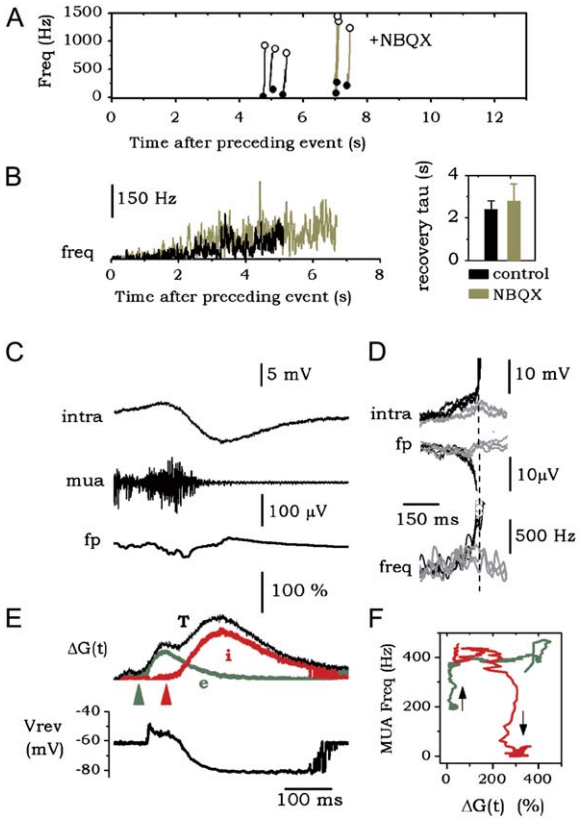

Figure 5. Effect of Reducing Excitatory Synaptic Efficacy

(A) Frequency changes during the buildup period plotted for three successful bursts in control conditions and in the presence of NBQX. NBQX (0.2–0.7 µM) increased the interevent interval ($p < 0.0001$). Filled circles indicate the firing frequency preceding the buildup, and open circles indicate that at the onset of the population burst. (B) Recovery dynamics of multiunit firing was not modified in NBQX (left). Traces show mean firing rate at control and under NBQX from a typical experiment. Time constant of the recovery of multiunit firing frequency was similar under NBQX and control (right). Data from n = 7 minislices. (C) NBQX at 0.2–0.7 µM increased the proportion of partial events. Field potential deflections were correlated with firing transients during partial events. Simultaneous intracellular recordings showed a sequence of depolarization followed by hyperpolarization. (D) Partial events (gray) compared with the buildup period in intracellular record (top), field potential record (middle), and firing rate data (bottom). (E) Time course of conductance changes (ΔG, upper) and the composite reversal potential (*Vrev*, lower) during partial events in a representative experiment. Total conductance changes (T, black) are separated in their excitatory (e, green) and inhibitory (I, red) components. Arrowheads mark the onset of the excitatory (green) and the inhibitory (red) event. (F) Plot of the firing rate versus changes during the rising phase in both the excitatory (green) and inhibitory (red) conductance from another representative experiment. Arrows near each trace indicate the temporal direction. Note that population firing was strongly reduced as the inhibitory conductance increased. Error bars represent the mean ± SDM.

proportion of partial events decreased significantly at the expense of all-or-none bursts (Figures 6A and 6B). We also noted a reduction in the hyperpolarization following a burst in intracellular records after CGP. Altogether, these results suggest that population activity during partial events results from interactions between excitatory and delayed inhibitory synaptic signaling.

Firing Induced by Single Pyramidal Cells Can Exceed Threshold and Trigger Population Events

Our results suggest that both excitatory glutamatergic actions and delayed inhibitory signaling mediated by $GABA_B$ receptors contribute to initiation of population events. If there is a firing threshold for population bursting, increasing firing activity by discharging a single cell might exceed the threshold and accelerate or even initiate a burst (Miles and Wong, 1983).

The relation between single-cell firing, population activity, and burst initiation was examined in 15 CA3a cells. Single-cell firing was induced at an interval less than that between spontaneous population bursts (spontaneous interval 6.5 ± 1.3 s, test interval 5.6 ± 0.8 s; Figure 7A).

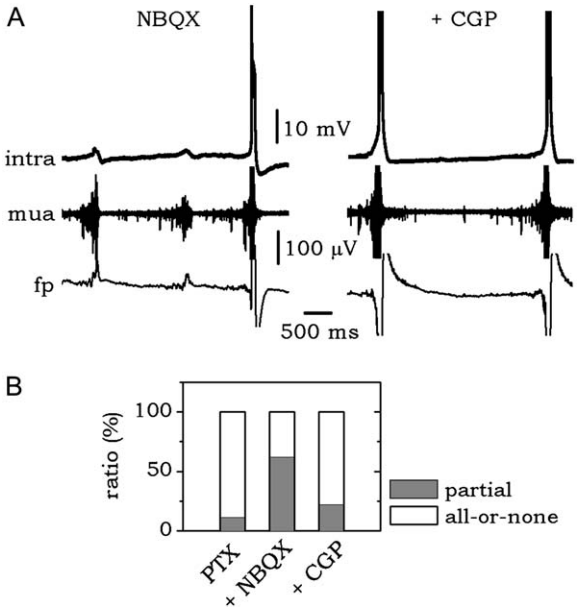

Figure 6. Effect of Blocking $GABA_B$ Receptors on Partial and All-or-None Population Activity

(A) Partial events occurred frequently, and all-or-none population events occurred less often in low concentrations of NBQX (0.4–0.7 μM). Adding the $GABA_B$ receptor blocker CGP52432 (2–4 μM) restored the situation where most events were all-or-none. Note the decrease of the after-hyperpolarization following population bursts after CGP.

(B) Proportion of partial and all-or-none population events before and after CGP52432. Data from n = 8 minislices.

We measured how often a population burst was triggered in the 200 ms after firing induced by 30 test stimuli. In 8 of 15 cells the probability was not higher than that of a chance coincidence (0.02–0.04). In seven cells, population events were initiated after multiunit firing induced by intracellular stimulation with a mean latency of 46 ± 32 ms and with a probability of 0.68 ± 0.27 (range 0.13–0.96). When an event was triggered, negative deflections were generated in field potential records (Figure 7B).

These data show that firing in some single pyramidal cells can initiate a recruitment process that leads to an all-or-none population burst. For the cells that could trigger population events, the peak frequency of multiunit activity when an event was initiated was significantly higher than that when an event was not initiated (Figures 7B and 7C). It was similar to that preceding spontaneously occurring population bursts (Figures 7D and 7E). Also, stimulating single cells more frequently (1 Hz) substantially reduced the interevent interval (Figure 7F). These data show that when population firing induced by a single pyramidal cell exceeded a threshold, a burst was initiated (Figure 7E).

Discussion

We have examined cellular and synaptic processes that govern the initiation of population bursts in disinhibited minislices of the CA3 region. Our data suggest that the precise timing of all-or-none bursts depends on active processes initiated after recovery from a previous burst. Several factors suggest that a threshold firing frequency must be exceeded to initiate population bursts. First, the firing rate was higher just before a burst than at any other point between population events (Figure 3). This increase in neuronal firing was associated with an acceleration of EPSPs in CA3a cells and a characteristic local field potential (Figure 1). Second, this collective activity could be modulated in both directions. Population bursts were advanced in time by injecting activity from a single cell into the network (Figure 7). In contrast, reducing either cellular excitability (Figure 4) or the efficacy of excitatory synapses abolished population bursts. Smaller reductions in synaptic efficacy revealed subthreshold partial events. They involved simultaneous firing of a subset of cells and were terminated by delayed inhibitory conductances mediated by $GABA_B$ receptors (Figures 5 and 6). Thus, threshold behavior may result from competition between excitatory synaptic actions and a delayed inhibitory feedback. Possibly similar threshold processes are involved in the generation of population bursts such as GDPs (Menendez de la Prida and Sanchez-Andres, 1999; Ben-Ari, 2001), human interictal-like activity (Cohen et al., 2002), and hippocampal sharp waves (Buzsaki et al., 1983).

Reconciling the Recovery and the Threshold Hypothesis

Hippocampal population bursts occur periodically. During the cycle between bursts in disinhibited slices, we detected three phases of population firing: (1) a recovery from the previous burst, (2) a plateau period of fluctuating activity after recovery, and (3) a buildup period of 50–150 ms when firing accelerates just before a burst (Figure 2). The plateau and buildup periods are not compatible with a population rhythm that depends exclusively on recovery processes.

Work on population bursts induced by high potassium concluded that the recovery period corresponds exclusively to the recovery of availability of excitatory transmitter after vesicle depletion induced by a previous population event (Bains et al., 1999; Staley et al., 1998). This model implies that the duration of an event should be correlated with the preceding interevent interval (Grzywacz and Sernagor, 2000; Tabak et al., 2001). We observed such a positive correlation at elevated values of potassium (8 mM), but not at lower levels (4 and 6 mM). Changes in external K^+ might affect vesicle dynamics (Stevens and Wesseling, 1999; Sara et al., 2002) and passive properties, and therefore also affect recovery time course (Staley et al., 1998).

Increasing cellular excitability reduced the plateau period of population activity so that recovery processes occupied a larger part of the interval between bursts. Even so, a buildup period of accelerating population firing was still evident at 8 mM K^+. Both intracellular and field records suggest that the buildup corresponds to an increase in synaptic traffic that occurs over several tens of milliseconds. It appears to emerge stochastically from the plateau period and to be generated in the CA3a region. Thus, recovery over a period of several seconds is needed before the next population burst can occur. However, the precise timing of the population bursts depends on active processes involving a sudden increase

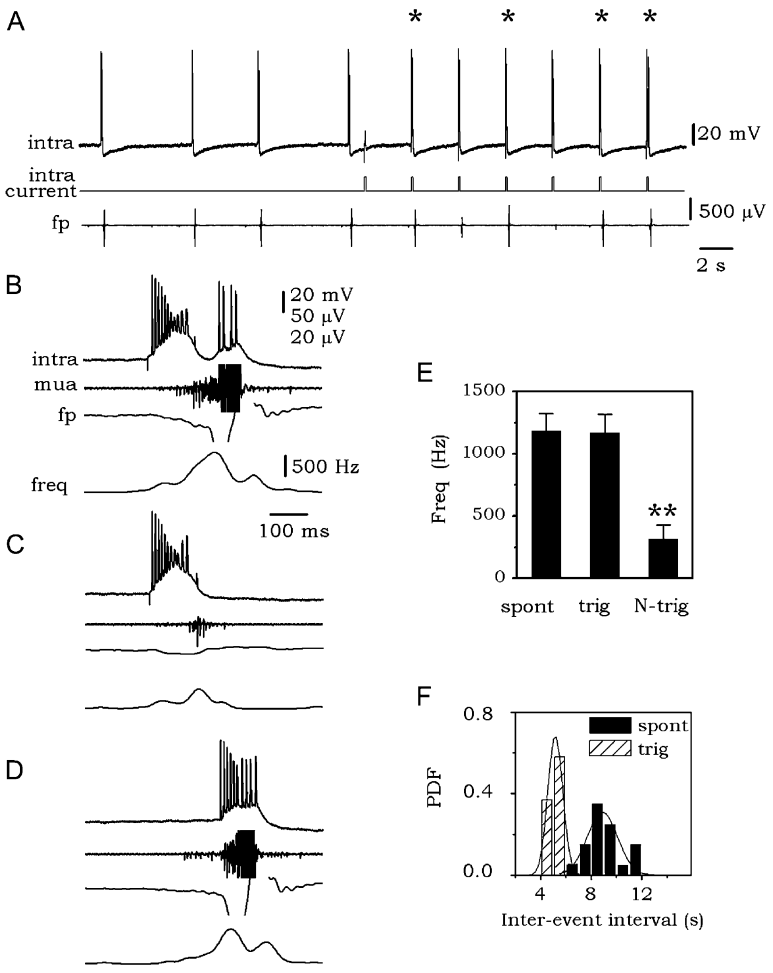

Figure 7. Population Activity Induced by One Pyramidal Cell Can Exceed the Threshold

(A) All-or-none population bursts occurred spontaneously at intervals in the range 4.1–7.9 s. Intracellular stimuli were delivered to induce burst firing at intervals of 5 s in one cell. Thirty of thirty-six intracellular bursts were followed at latency 55 ± 11 ms by a population burst (*). Traces are intracellular potential, injected current, and field potential. (B) Cellular burst followed by a population burst. (C) Cellular burst not followed by a population burst. (D) Spontaneous population burst. (E) The frequency of extracellular firing when a population burst was triggered by intracellular firing was close to that occurring just before a spontaneous population event. The peak frequency of population firing induced by pyramidal cell firing was lower when a population burst was not triggered. Mean values from at least 30 trials and 30 spontaneous events (n = 7 pyramidal cells). (F) Interevent intervals before (black) and after (dashed) stimulation of one cell. Error bars represent the mean ± SDM.

in CA3a cell firing mediated by recurrent excitatory synapses (Traub and Miles, 1991; Wenner and O'Donovan, 2001; Latham et al., 2000).

The threshold firing frequency at the burst onset was higher than during any transient increase in firing during the cycle between bursts, pointing to threshold behavior. We note that the threshold values given here all refer to multiunit firing derived from a single electrode. As for action potentials generated by a single neuron (Jack et al., 1983; Fricker et al., 1999), it may be difficult to define the threshold for an all-or-none network event precisely. The exact network threshold may lie between the highest frequency associated with a partial event (450–500 Hz) and the lower frequency at the burst onset (750–800 Hz). Probably the threshold is exceeded during the later stages of the buildup period at a point corresponding to an unstable condition that is difficult to identify from either the field potential or firing frequency (Tabak et al., 2001; Latham et al., 2000).

When excitatory synaptic efficacy was reduced, partial population events accompanied by small field potentials occurred more frequently (Figure 5). Intracellularly, they were correlated with a sequence of glutamatergic excitation and inhibition mediated by $GABA_B$ receptors. Our analysis of conductance changes associated with partial events suggests that $GABA_B$ inhibitory conductances were recruited after the onset of excitatory events (Figure 5E). However, their latencies were short enough that they could curtail population firing. While our data suggest that postsynaptic $GABA_B$-mediated inhibition is crucial in terminating population firing, presynaptic actions of the same receptors may also be involved. GABA actions at presynaptic $GABA_B$ receptors would tend to reduce liberation at glutamatergic synapses and so contribute to burst termination (Staley et al., 1998).

The time course of the $GABA_B$-mediated conductance suggests that interneurons discharge during the buildup period. We confirmed this point with cell-attached records (Figure S4) showing that both interneurons and pyramidal cells fired before the onset of the population burst. This situation differs from the synchronous activity induced in the subiculum by exposure to zero Mg^{2+}, where inhibitory cells tend to fire after glutamatergic cells (Menendez de la Prida and Gal, 2004), but resembles the CA1 population bursts induced by high potassium, where some interneurons also fire before pyramidal cells (Aradi and Maccaferri, 2004). Cell-attached recordings revealed variability in the firing of pyramidal cells during the buildup to successive bursts. Some cells in the CA3a area never discharged during the buildup period, while other cells fired before some but

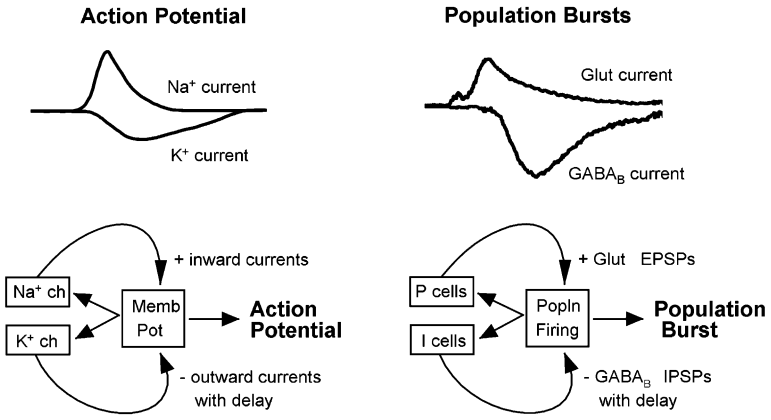

Figure 8. Diagram of Positive and Negative Feedback Processes Controlling Threshold Behavior in Action Potential Generation by Single Neurons and Population Burst Initiation

Synaptic events mediated by glutamatergic transmission may play a positive feedback role analogous to that of Na^+ currents in the initiation of an action potential. $GABA_B$-mediated synaptic events contribute a negative feedback equivalent to that of K^+ currents in a single neuron.

not all population events. Thus, the driver function is distributed across the population and can be most clearly described with multicellular recordings.

Initiating Events within the Driver CA3a Region

The processes that initiate a population event seem to be limited to the CA3a region (Colom and Saggau, 1994; Knowles et al., 1987; Traub and Wong, 1982). We detected a field potential in this region, but not in the follower CA3b/c areas, and observed an acceleration of EPSC frequency in CA3a cells, but not in CA3b/c neurons. Distinct cellular and morphological properties of cells in this region may explain their pacemaker function (Masukawa et al., 1982).

A local buildup suggests that a few neurons can initiate a burst. Indeed, we showed that activity in some single cells could increase population firing to suprathreshold frequencies and advance the timing of a population burst (Figure 7). Recent data suggest that firing in single cortical pyramidal cells can have behavioral effects even in the normally inhibited brain. Trains of action potentials in motor cortex cells initiate whisker movements (Brecht et al., 2004) with latencies of 50–100 ms. Such long latencies would permit the recruitment of other cortical pyramidal cells via recurrent circuits by similar mechanisms as described here.

How are population bursts generated within a neuronal network linked by excitatory synapses? Single cells are recruited to the burst when depolarized to their *action potential threshold*. Recruitment depends on the summation of EPSPs initiated by multiple presynaptic cells firing during a restricted time. Summing this process across the population implies the existence of a *network firing threshold*. Such a network threshold imposes a frequency condition, since a critical number of cells must fire synchronously before $GABA_B$-mediated conductances suppress firing (Figure 5; Menendez de la Prida and Gal, 2004).

We suggest that the critical number of cells fire simultaneously by chance. This would explain why changes in synaptic transmission but not in cellular excitability modify the frequency threshold. When synaptic efficacy was reduced by NBQX, more EPSPs were needed to reach action potential threshold and to trigger a population event. This correlates with the higher firing rate during partial events and longer buildup period. In contrast, the increase in cellular excitability induced by high potassium increases the probability that stochastic fluctuations of firing rate exceed a frequency threshold and so reduces the interval between population events. However, the buildup period was not reduced in high potassium. Possibly the frequency of excitatory synaptic events during the buildup is not significantly increase because contributing cells are already active. Alternatively, inhibitory synaptic inputs are also enhanced, resulting in an unchanged buildup period (Aradi and Maccaferri, 2004).

A Threshold Is a Threshold

Are there analogies between threshold processes in the initiation of a neuronal population bursts and other all-or-none biological events? One obvious parallel is the threshold behavior in the generation of an action potential by a neuron. Action potential discharge can occur if Na^+ channels open fast enough to depolarize a cell to threshold before K^+ channels with slower kinetics can prevent further depolarization (Jack et al., 1983). Opening of both Na^+ and K^+ channels depends on membrane potential.

We suggest that formal similarities exist with the threshold behavior we have described in neuronal population activity (Figure 8). Population firing may correspond to membrane potential. Glutamatergic synaptic events would be analogous to Na^+ channel openings in that their frequency depends on population firing and that they act to enhance firing in a positive feedback fashion. In contrast, $GABA_B$-mediated synaptic events may be analogous to K^+ channel openings in that they depress population firing with a delay due to the G protein coupling between receptor activation and channel opening. The threshold condition emerges since activity must spread through the network via glutamatergic transmission at divergent recurrent excitatory connections fast enough that $GABA_B$-mediated inhibition cannot stop the spread. Clearly other cellular and network processes such as connectivity, synaptic efficacy, and EPSP-spike coupling will affect how the population approaches its firing threshold. Further theoretical and experimental work is needed to pursue analogies between these threshold processes.

Experimental Procedures

Slice Preparation

Slices from the middle third of the hippocampus were prepared according to European regulations (86/609/EEC) from guinea pigs (weight 100–200 g) anesthetized by i.p. injection of chloral hydrate (800 mg/kg). Animals were perfused intracardially with a cold (3ºC–5ºC) solution consisting of the following: 26 mM $NaHCO_3$, 1 mM KCl, 10 mM $MgCl_2$, 1 mM $CaCl_2$, 248 mM sucrose, and 10 mM glucose, equilibrated with 5% CO_2 in 95% O_2, and were killed by decerebration. Minislices containing the CA2 and CA3 regions were prepared using dissection scissors. Minislices were transferred to either an interface or submerged recording chamber at 34ºC–35ºC, perfused with a solution containing the following: 124 mM NaCl, 26 mM $NaHCO_3$, 4–8 mM KCl, 2 mM $MgCl_2$, 2 mM $CaCl_2$ and 10 mM glucose and equilibrated with 5% CO_2 in 95% O_2. The $GABA_A$ receptor antagonist PTX (Sigma) was added to the ACSF, usually at 100 μM. NBQX and CGP52432 from Sigma were added to the ACSF at different concentrations.

Extracellular and Intracellular Sharp Recordings

Extracellular recording electrodes were made from tungsten wire of 50 μm diameter, etched to a diameter of 2–6 μm electrolytically (1–5 V AC for 1–2 min, 5 M KNO_2) under visual control. Electrodes were insulated by applying varnish to within ~200 μm of their tip (final resistance 500–1000 kΩ). Up to four metal electrodes were mounted on separate holders and placed in the s. pyramidale. Potential differences between tungsten electrodes and a reference Ag-AgCl electrode were amplified 1000 times and band-pass filtered at 0.1 Hz–10 kHz (AM Systems). Signals were stored on a modified videotape recorder (Neurodata, New York) and digitized using a 12-bit, 16-channel A-D converter (Digidata 1200A, Axon Instruments). Intracellular sharp records were obtained using glass microelectrodes filled with 2 M potassium acetate (electrode resistance: 40–80 MΩ). Membrane potential was measured using an Axoclamp 2B amplifier. Sharp recordings (n = 45) were obtained from the s. pyramidale of the CA3 subregion. Only cells with stable membrane potentials negative to −60 mV, overshooting action potentials, and input resistance > 20 MΩ were considered.

Patch Recordings

Visual and blind somatic patch recordings (n = 16) were obtained using an Axoclamp 2B amplifier. Patch pipettes were filled with either Cs- or K-based solutions. The composition of the K-based solution was 113 mM K-gluconate, 6 mM KCl, 1 mM $MgCl_2$, 1 mM NaCl, 1 mM EGTA, 5 mM HEPES, 2 mM K_2ATP, 0.3 mM NaGTP, pH 7.3 adjusted with KOH and osmolarity between 290 and 300 mOsm. The Cs-based solution contained 115 mM Cs-gluconate, 4 mM $MgCl_2$, 1 mM EGTA, 5 mM HEPES, 2 mM Na_2ATP, 0.3 mM NaGTP, pH 7.3 adjusted with CsOH and osmolarity between 290 and 300 mOsm. EPSCs were recorded in voltage clamp at a holding potential of −85 mV using the Cs-based solution. Synaptic activity associated with partial events was recorded in voltage clamp using the K-based solution. Cell-attached recordings were obtained using pipettes filled with either the Cs- or the K-based solutions. Patch pipettes had a resistance of 4–6 MΩ. Capacitance compensation and bridge balance were performed before patching. The access resistance was calculated offline from the cell response to subthreshold current pulses (double exponential fitting). The junction potential (−7 mV for K-based solution and −10 mV for Cs-based solution) was corrected.

Data and Statistical Analysis

Signals were processed with routines written in LabView (National Instruments) and Matlab (MathWorks). Distinct frequency components were separated with digital Bessel filters. Action potentials were detected using an up-only algorithm that retains positive deflection to introduce no time delay (Cohen and Miles, 2000). The timing of extracellular units was measured to derive a continuous rate signal by convolving the timing of each detected event with a Gaussian function of variable standard deviation (Szucs, 1998). We typically used a standard deviation of 10 ms to obtain a nearly instantaneous firing rate. No attempt was made to distinguish between units generated by pyramidal cells and interneurons. EPSCs were detected using the Mini Analysis Program (Synaptosoft Inc.) and verified visually. Latencies between different electrodes were calculated using cross-correlation analysis of the field potentials. Event onset was defined from the fast slope of the field potential and from cross-correlation analysis.

Results are given as mean ± SD. Results were compared using Student's t test or the ANOVA test at $p < 0.05$. Precise p values are indicated in every case, except when $p < 0.0001$. Simple linear regression was performed with a confidence interval of 95%.

Estimation of Synaptic Conductances during Partial Population Events

Changes in membrane conductance (ΔG) and the composite reversal potential (*Vrev*) were calculated following the method of Borg-Graham et al. (1998). Synaptic responses during partial population events were evaluated from current-clamp records derived from sharp electrodes or from voltage-clamp data obtained from whole-cell recordings at three or four different membrane potentials. Data from both sets were pooled as no difference was found in the *Vrev* values and the relative dynamics of the excitatory and the inhibitory components. Continuous estimation of ΔG and *Vrev* were obtained from the linear regression (95% confidence interval) of the I-V plot at the sampling rate. Membrane potential was corrected for the drop across access resistance, which was lower than 78 MΩ and 35 MΩ for sharp and patch recordings, respectively. The relative conductance increase $\Delta G(t)$ was given as $(G(t) - Grest)/Grest$ in percent, where *Grest* is the resting conductance. Dissection of the excitatory and the inhibitory components of the composite synaptic event was made with the following formulas (Borg-Graham, 2001):

$$\Delta Ge = \Delta G \cdot (Vrev - Vi)/(Ve - Vi)$$

$$\Delta Gi = \Delta G \cdot (Vrev - Ve)/(Vi - Ve)$$

where *Ve* and *Vi* are the reversal potential of glutamatergic (+10 mV) and $GABA_B$-mediated synaptic currents (see Borg-Graham, 2001 for further details). For data obtained with sharp electrodes, *Vi* was set at −85 mV. For data obtained using patch, *Vi* was calculated from the Nernst equation according to the extracellular and intracellular K^+ concentration. We note that conclusions from this analysis are more relevant for processes taking place at the soma and proximal dendrites. We cannot exclude distortions caused by less visible dendritic inputs neither from poorly clamped voltage-dependent dendritic channels.

Minimizing Spurious Cross-Correlation and Unit Detection from Extracellular Records

We determined the minimum separation of two electrodes that would avoid unit oversampling. In four minislices, we performed cross-correlation analysis of activity detected by two electrodes separated by variable distances along the s. pyramidale. When two electrodes were separated by ~200 μm or more, oversampling did not occur (Figure S1). This minimal separation is close to a previous estimate that an extracellular electrode detects activity from cells lying within a radius of 80–100 μm (Cohen and Miles, 2000).

On the Accuracy of Measurements of Action Potential and EPSC Frequency

In extracellular records from multiple units, spike overlaps may occur and detection algorithms may underestimate firing frequency. We first simulated independently occurring action potentials to determine the detection limit of our method. The detection algorithm could resolve two spikes separated by >0.4–0.8 ms (Figure S3A). This limiting interval (ΔT) should increase as more overlapping occurs. This was examined in simulations of 100–200 spikes at intervals that followed a Gaussian distribution with mean frequencies from 100 to 1200 Hz (Figure S3B). We found that the detected frequency deviated from the expected frequency for values higher than 700 Hz (Figure S3C). Beyond this cutoff, overlapping spikes may lead to underestimates of firing frequencies. However, the distortion of the original probability distribution function (Figure S3D) may be corrected numerically if the following condition of convergence is fulfilled (Ankri and Korn, 1999):

$$freq \cdot \Delta T < \exp(-1)$$

In our case, for an overlapping window $\Delta T = 0.4$ ms, we could correct for *freq* < 919 Hz. Further, since recurrent excitatory synaptic interactions occur, we cannot assume that spike timing is independent in the period preceding population events and could reach values larger than the detection limit. Therefore, we also used data from spike visual counting from intervals of 10 ms, similar to that used for convolution in the automatic detection algorithm. Similar issues of event detection emerge in overlapping EPSCs during the buildup period (Ankri and Korn, 1999). For EPSC analysis, we estimate an overlapping window of 1.1 ms, corresponding to a detection limit of 334 Hz.

Supplemental Data

The Supplemental Data include four supplemental figures and can be found with this article online at http://www.neuron.org/cgi/content/full/49/1/131/DC1/.

Acknowledgments

We thank Joel Tabak, Michael Hausser, and Roger D. Traub for useful comments. This work was supported by a short-term fellowship from the Human Frontier Science Program, the Programa Ramón y Cajal from the Spanish Ministry of Education and Science, and grants from the Spanish Ministry of Education and Science (BFI2003-04305) and Comunidad de Madrid (GR/SAL/0131/2004) to L.M.P., and by an Action Concertée Incitative (French Ministère de l'Education Nationale de l'Enseignement Superieure et de la Recherche), INSERM, and the NIH (MH54671) to R.M.

Received: April 18, 2005
Revised: August 29, 2005
Accepted: October 20, 2005
Published: January 4, 2006

References

Agmon, A., and Wells, J.E. (2003). The role of the hyperpolarization-activated cationic current I(h) in the timing of interictal bursts in the neonatal hippocampus. J. Neurosci. *23*, 3658–3668.

Alger, B.E., and Nicoll, R.A. (1980). Epileptiform burst afterhyperpolarization: calcium-dependent potassium potential in hippocampal CA1 pyramidal cells. Science *210*, 1122–1124.

Ankri, N., and Korn, H. (1999). A statistical method for correcting distortions of amplitude distribution histograms due to collisions of synaptic events. J. Neurosci. Methods *91*, 83–99.

Aradi, I., and Maccaferri, G. (2004). Cell type-specific synaptic dynamics of synchronized bursting in the juvenile CA3 rat hippocampus. J. Neurosci. *24*, 9681–9692.

Ayala, G.F., Dichter, M., Gumnit, R.J., Matsumoto, H., and Spencer, W.A. (1973). Genesis of epileptic interictal spikes. New knowledge of cortical feedback systems suggests a neurophysiological explanation of brief paroxysms. Brain Res. *52*, 1–17.

Bains, J.S., Longacher, J.M., and Staley, K.J. (1999). Reciprocal interactions between CA3 network activity and strength of recurrent collateral synapses. Nat. Neurosci. *2*, 720–726.

Ben-Ari, Y. (2001). Developing networks play a similar melody. Trends Neurosci. *24*, 353–360.

Ben-Ari, Y., Cherubini, E., Corradetti, R., and Gaiarsa, J.L. (1989). Giant synaptic potentials in immature rat CA3 hippocampal neurones. J. Physiol. *416*, 303–325.

Borg-Graham, L.J. (2001). The computation of directional selectivity in the retina occurs presynaptic to the ganglion cell. Nat. Neurosci. *4*, 176–183.

Borg-Graham, L.J., Monier, C., and Fregnac, Y. (1998). Visual input evokes transient and strong shunting inhibition in visual cortical neurons. Nature *393*, 369–373.

Bragin, A., Jando, G., Nadasdy, Z., Hetke, J., Wise, K., and Buzsaki, G. (1995). Gamma (40–100 Hz) oscillation in the hippocampus of the behaving rat. J. Neurosci. *15*, 47–60.

Brecht, M., Schneider, M., Sakmann, B., and Margrie, T.W. (2004). Whisker movements evoked by stimulation of single pyramidal cells in rat motor cortex. Nature *427*, 704–710.

Buzsaki, G. (1986). Hippocampal sharp waves: their origin and significance. Brain Res. *398*, 242–252.

Buzsaki, G., Leung, L.W., and Vanderwolf, C.H. (1983). Cellular bases of hippocampal EEG in the behaving rat. Brain Res. *287*, 139–171.

Calvin, W.H. (1972). Synaptic potential summation and repetitive firing mechanisms: input-output theory for the recruitment of neurons into epileptic bursting firing patterns. Brain Res. *39*, 71–94.

Chamberlin, N.L., Traub, R.D., and Dingledine, R. (1990). Role of EPSPs in initiation of spontaneous synchronized burst firing in rat hippocampal neurons bathed in high potassium. J. Neurophysiol. *64*, 1000–1008.

Cohen, I., and Miles, R. (2000). Contributions of intrinsic and synaptic activities to the generation of neuronal discharges in in vitro hippocampus. J. Physiol. *524*, 485–502.

Cohen, I., Navarro, V., Clemenceau, S., Baulac, M., and Miles, R. (2002). On the origin of interictal activity in human temporal lobe epilepsy in vitro. Science *298*, 1418–1421.

Colom, L.V., and Saggau, P. (1994). Spontaneous interictal-like activity originates in multiple areas of the CA2-CA3 region of hippocampal slices. J. Neurophysiol. *71*, 1574–1585.

Fedirchuk, B., Wenner, P., Whelan, P.J., Ho, S., Tabak, J., and O'Donovan, M.J. (1999). Spontaneous network activity transiently depresses synaptic transmission in the embryonic chick spinal cord. J. Neurosci. *19*, 2102–2112.

Fricker, D., Verheugen, J.A., and Miles, R. (1999). Cell-attached measurements of the firing threshold of rat hippocampal neurones. J. Physiol. *517*, 791–804.

Garaschuk, O., Linn, J., Eilers, J., and Konnerth, A. (2000). Large-scale oscillatory calcium waves in the immature cortex. Nat. Neurosci. *3*, 452–459.

Grzywacz, N.M., and Sernagor, E. (2000). Spontaneous activity in developing turtle retinal ganglion cells: statistical analysis. Vis. Neurosci. *17*, 229–241.

Hablitz, J.J. (1984). Picrotoxin-induced epileptiform activity in hippocampus: role of endogenous versus synaptic factors. J. Neurophysiol. *51*, 1011–1027.

Ives, A.E., and Jefferys, J.G. (1990). Synchronization of epileptiform bursts induced by 4-aminopyridine in the in vitro hippocampal slice preparation. Neurosci. Lett. *112*, 239–245.

Jack, J.J.B., Noble, D., and Tsien, R.W. (1983). Electric Current Flow in Excitable Cells (Oxford: Oxford University Press).

Jefferys, J.G. (1994). Experimental neurobiology of epilepsies. Curr. Opin. Neurol. *7*, 113–122.

Knowles, W.D., Traub, R.D., and Strowbridge, B.W. (1987). The initiation and spread of epileptiform bursts in the in vitro hippocampal slice. Neuroscience *21*, 441–455.

Latham, P.E., Richmond, B.J., Nelson, P.G., and Nirenberg, S. (2000). Intrinsic dynamics in neuronal networks. I. Theory. J. Neurophysiol. *83*, 808–827.

Leung, L.S. (1992). Fast (beta) rhythms in the hippocampus: a review. Hippocampus *2*, 93–98.

Levy, R., Hutchison, W.D., Lozano, A.M., and Dostrovsky, J.O. (2000). High-frequency synchronization of neuronal activity in the subthalamic nucleus of parkinsonian patients with limb tremor. J. Neurosci. *20*, 7766–7775.

Masukawa, L.M., Benardo, L.S., and Prince, D.A. (1982). Variations in electrophysiological properties of hippocampal neurons in different subfields. Brain Res. *242*, 341–344.

Menendez de la Prida, L., and Gal, B. (2004). Synaptic contributions to focal and widespread spatiotemporal dynamics in the isolated rat subiculum in vitro. J. Neurosci. *24*, 5525–5536.

Menendez de la Prida, L., and Sanchez-Andres, J.V. (1999). Nonlinear frequency-dependent synchronization in the developing hippocampus. J. Neurophysiol. *82*, 202–208.

Menendez de la Prida, L., and Sanchez-Andres, J.V. (2000). Heterogeneous populations of cells mediate spontaneous synchronous bursting in the developing hippocampus through a frequency-dependent mechanism. Neuroscience *97*, 227–241.

Miles, R., and Wong, R.K. (1983). Single neurones can initiate synchronized population discharge in the hippocampus. Nature *306*, 371–373.

Miles, R., and Wong, R.K. (1987). Inhibitory control of local excitatory circuits in the guinea-pig hippocampus. J. Physiol. *388*, 611–629.

Sara, Y., Mozhayeva, M.G., Liu, X., and Kavalali, E.T. (2002). Fast vesicle recycling supports neurotransmission during sustained stimulation at hippocampal synapses. J. Neurosci. *22*, 1608–1617.

Schwartzkroin, P.A., and Prince, D.A. (1978). Cellular and field potential properties of epileptogenic hippocampal slices. Brain Res. *147*, 117–130.

Somogyi, P., and Klausberger, T. (2005). Defined types of cortical interneurone structure space and spike timing in the hippocampus. J. Physiol. *562*, 9–26.

Staley, K.J., Longacher, M., Bains, J.S., and Yee, A. (1998). Presynaptic modulation of CA3 network activity. Nat. Neurosci. *1*, 201–209.

Staley, K.J., Bains, J.S., Yee, A., Hellier, J., and Longacher, J.M. (2001). Statistical model relating CA3 burst probability to recovery from burst-induced depression at recurrent collateral synapses. J. Neurophysiol. *86*, 2736–2747.

Steriade, M. (2005). Sleep, epilepsy and thalamic reticular inhibitory neurons. Trends Neurosci. *28*, 317–324.

Stevens, C.F., and Wesseling, J.F. (1999). Identification of a novel process limiting the rate of synaptic vesicle cycling at hippocampal synapses. Neuron *24*, 1017–1028.

Szucs, A. (1998). Applications of the spike density function in analysis of neuronal firing patterns. J. Neurosci. Methods *81*, 159–167.

Tabak, J., Rinzel, J., and O'Donovan, M.J. (2001). The role of activity-dependent network depression in the expression and self-regulation of spontaneous activity in the developing spinal cord. J. Neurosci. *21*, 8966–8978.

Traub, R.D., and Dingledine, R. (1990). Model of synchronized epileptiform bursts induced by high potassium in CA3 region of rat hippocampal slice. Role of spontaneous EPSPs in initiation. J. Neurophysiol. *64*, 1009–1018.

Traub, R.D., and Miles, R. (1991). Neuronal Networks of the Hippocampus (New York: Cambridge University Press).

Traub, R.D., and Wong, R.K. (1982). Cellular mechanism of neuronal synchronization in epilepsy. Science *216*, 745–747.

Traub, R.D., Whittington, M.A., Stanford, I.M., and Jefferys, J.G. (1996). A mechanism for generation of long-range synchronous fast oscillations in the cortex. Nature *383*, 621–624.

Wenner, P., and O'Donovan, M.J. (2001). Mechanisms that initiate spontaneous network activity in the developing chick spinal cord. J. Neurophysiol. *86*, 1481–1498.